Sintering of Small Particles

by

Jonathan Paras

Submitted to the
Department of Materials Science and Engineering
in Partial Fulfillment of the Requirements for the Degree of

Bachelor of Science

at the

Massachusetts Institute of Technology

June 2018

Signature redacted

Signature of author .....

Jonathan Paras
Department of Materials Science and Engineering
April 27th , 2018

Signature redacted

Certified by .....

Christopher A. Schuh
Danae and Vasilis Salapatas Professor of Metallurgy
Thesis Supervisor

Signature redacted

Accepted by.....

JueJun Hu
Associate Professor Materials Science and Engineering
Chairman, Undergraduate Thesis Committee

Sintering of Small Particles

By

Jonathan Paras

Submitted to the Department of Materials Science and Engineering
On 4/27/2018 in Partial Fulfillment of the
Requirements for the Degree of Bachelor of Science in
Materials Science and Engineering

ABSTRACT

An atomistic approach to modeling the sintering of nanocrystalline alloys has been developed. It has been shown that there exist alloys that exhibit both nanostructured stability and undergo an accelerated sintering process [1], [2]. However, the widespread adoption of such alloys has been limited by a lack of understanding of the processing kinetics that lead to the accelerated sintering phenomena. To better understand the role of surface diffusion, and the effect that system enthalpies of mixing have on inter-particle neck formation, a 3D kinetic monte carlo (KMC) model was proposed to study these phenomena. The results of these simulations demonstrate that positive enthalpy of mixing highlighted as a necessary criterion for nanocrystalline stability in [1], also leads to the fast diffusing elements ability to form the inter-particle neck. The condition of lower temperature neck formation by fast diffusing alloy elements is hypothesized to be the mechanism behind which accelerated sintering occurs. The findings in this paper demonstrate that positive enthalpy of mixing alloys can be designed to sinter at lower temperatures and shorter cycle durations if they have adequate solute present on the surface of the particle.

Thesis Supervisor: Christopher Schuh

Title(s): Department Head, Danae and Vasilis Salapatas Professor of Metallurgy

Acknowledgements

I would first like to thank both Dr. Arvind Kalidindi and Thomas Hardin for their mentorship and expertise. From the simple question of how to compile a program in Linux onwards to more complicated questions about C++ programing and alloy thermodynamics, both of you were extraordinarily patient. Patience that never flinched even when I was concerned about my own graduation. I would also like to extend my thanks to the rest of the members of the Schuh group for putting up with the *de facto* Chief UROP as he tried to become a real scientist.

I would like to thank Professor Christopher Schuh for being an enthusiastic mentor. He pushed me to do something that I initially had no experience in (and was rather terrified about) and continued to remind me that the most interesting answers to scientific questions often sit behind a mound of hard work. To paraphrase our meetings, this is a good start!

I would like to thank my friend, Ethan Witt, during the early days of my programming for helping me debug all the rookie mistakes I made while learning to program. I told you that Course 3 undergraduates can learn to do what you do, just not as well.

Finally, I would like to thank all my family and friends. Emotional support is often a less visible part of every success story. I would not have made it this far without you Mom, Dad, and Steph. And to you, Catherine, you remain the only good reason to leave the lab.

Table of Contents

List of Figures

List of Tables

1 Introduction

1.1 Motivation

Nanocrystalline metal alloys exhibit superior mechanical properties when compared to their coarse-grained counterparts[3]–[7]. These properties include improved hardness, ductility, and most importantly, yield strength. The nature of these properties has generated significant academic research interest[4], [8]–[10]. Nanocrystalline alloys have also demonstrated immediate industrial potential for future light-weighting and mechanically demanding applications [7].

However, widespread adoption of these alloys has been hampered by the inability to synthesize bulk samples, due to a lack of thermal stability inherent in nanocrystalline systems. Recent research has identified both an alloying technique and accompanying processing method to produce stable nanocrystalline alloys [11]–[15]. These works identified alloys that decrease the free energy of grain boundaries by forming a second solute rich phase during sintering

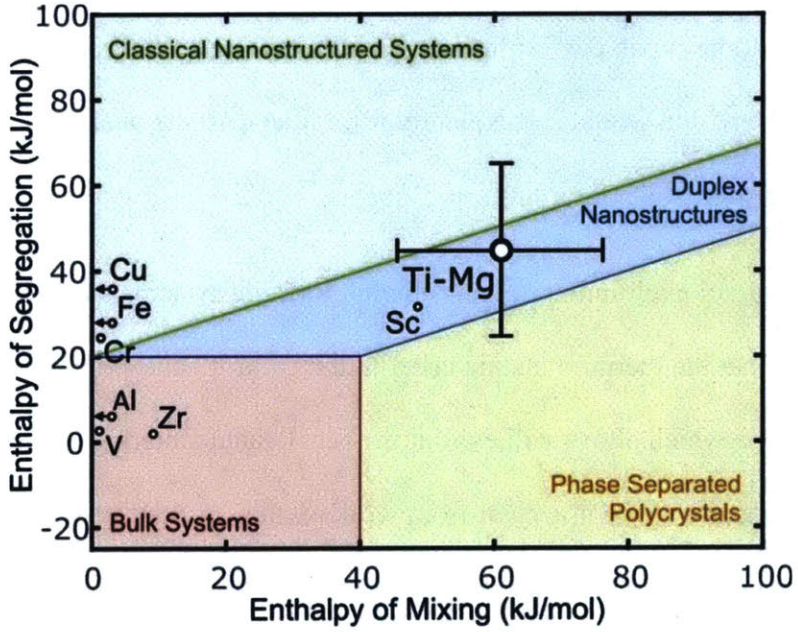

Figure 1: Nanocrystalline alloy stability map provided from references [11]-[15] for various enthalpy of segregation of solute and enthalpy of mixing values

coupled with solute preferentially segregating to the grain boundaries. This particular configuration, known as a "nano-duplex", forms under a specific range of thermodynamic criteria and is highlighted in Figure 1 above [1].

It was discovered that some of the alloys that were predicted to form a nano-duplex with stable nanocrystalline structure exhibit sintering at lower temperatures and for shorter cycle durations[16], [17]. This was dubbed "accelerated sintering" and W-Cr represented a leap in the ability to produce bulk nanocrystalline alloys through the sintering process. Alloys of this type are mechanically alloyed [18] and sintered in the solid state. These works verified that accelerated sintering scheme only worked in positive enthalpy of mixing systems that formed stable nanocrystalline grains. Systems that had positive enthalpies of mixing but coarsened easily during processing, or systems that had stable nanocrystalline grains but were negative enthalpy of mixing systems, did not exhibit accelerated sintering [19].

It was hypothesized in the works cited above the nanocrystallinity provided a dense grain boundary network with which low temperature diffusion of solute could easily be activated. From here they would be capable of surface segregation owing to their positive enthalpy of mixing with the solvent and would subsequently form inter-particle necks at lower processing temperatures and shorter cycle durations.

Further experimental exploration of nano-duplex forming systems such as Ti-Mg and Fe-Au have demonstrated that the thermodynamic criteria that control nano-duplex formation do not sufficiently determine which alloys will exhibit the accelerated sintering necessary to limit coarsening during densification. It is clear from work on these model systems and others [16] that a kinetic requirement exists that acts as a tighter constraint on accelerated sintering than the thermodynamic requirements for nano-duplex formation. However, such a requirement appears

to remain intrinsically linked with both the nanocrystallinity of the alloy's microstructure and a positive enthalpy of mixing regime. The difficulty in developing an analytical criterion for the kinetics of accelerated sintering directly from experimental data has necessitated the use of system modeling to help develop the necessary insight.

1.2 State of the Art Sintering Models

The objective of this work is to create a model that can provide insight into the kinetics under which accelerated sintering will occur in nano-duplex forming alloys. It has been noted that systems which exhibit accelerated sintering typically produce inter-particle necks that are predominantly solute, at lower temperatures than typical sintering would occur in the pure material.

It is hypothesized in [2] that during the sintering process of a nano-duplex alloy, the increased density of grain boundaries coupled with the segregation of the solute to grain boundary sites present a viable path for surface segregation of the solute to occur. This is then followed by migration of the solute from areas of high curvature (the particle surface) to areas of low curvature (inter-particle necks). To properly capture these phenomena, a complete sintering model will have to include alloy dynamics such as the system enthalpy of mixing, surface diffusion, as well as bulk and grain boundary diffusion and segregation events as mediated by vacancies.

Previous theoretical work has sought to study the sintering process through a variety of thermodynamic and analytical methods but no such models currently exist for nanocrystalline alloys during the sintering process The earliest techniques attempted to find constitutive

relationships between temperature, sintering duration, and powder compact density[20], [21]. These model's main weakness is that they were not capable of handling phase transformation as would be the case in a nano-duplex system undergoing sintering. Otherwise these are the most compelling models because they are easy for others to use.

Other analyses have used phase field models which attempt to minimize a thermodynamic potential in order to drive the microstructural evolution [22]–[24]. The main difficulty with this type of modeling technique is successfully linking the time units established in the overall free-energy function with those in the real world. This would make a discussion of accelerated sintering philosophically difficult if one were not capable of rigorously showing that under given kinetic conditions, accelerated sintering occurs more quickly in time. Nevertheless, these models have proven successful at handling multiple phases and reproducing morphologically correct sintering features including phase separation and coarsening.

Potts model metropolis codes have also been employed to similar effect by probing the configurational space for the lowest energy states [25], [26]. However, these techniques do not provide insight into the kinetics of the sintering process as neither metropolis nor phase field have established physical time links. Again, it would be difficult to make the claim of accelerated sintering without a comparison in real time. Metropolis Monte Carlo also represents a sampling of the configurational space according to Boltzman statistics. This will find equilibrium state of the system in configuration space, but does not capture the kinetics of such evolution even though simulation "steps" are taken.

A few molecular dynamic simulations have been conducted mainly serving to demonstrate the viability of using MD for longer time-scale processes, and have not been focused on probing the evolutionary kinetics of the sintering process with respect to composition [27].

Kinetic Monte Carlo (KMC) would represent a particularly suitable simulation method to probe the long-time evolution that occurs during the sintering process. Current modeling capability in this area is lacking, however, with papers attempting to use KMC Potts models for an analysis of the kinetics[25], [26], [28]. While Potts models have proven effective in developing morphologically correct grain and can capture the coarsening process, time in these models is represented as Monte Carlo steps (MCS). This is not real-world time, and as has been mentioned before, a metropolis algorithm implementing a Potts model samples configuration space and accepts or rejects moves based upon Boltzmann statistics. While systems may seem to evolve in MCS in a chronological manner, this merely proves that the evolution of configurational sampling follows a similar trajectory to the process in the real world, not that the chronology of these events are meaningfully linked to real world time.

There has been at least one simulation run with a simple KMC for sintering of gold nano-particles, but this work did not formalize how to treat alloying dynamics such as the enthalpy of mixing, nor did it provide a consistent way to incorporate different alloying system properties to allow the study of a broader range of materials [29].

As a first step in understanding nanocrystalline sintering, this thesis will seek to propose a model that consists of two particles on an 3D, FCC lattice. This model will include both surface and bulk diffusion mediated by vacancies on an identical lattice and use the KMC algorithm to establish a rigorous time link. The next objective would be to simulate particles with radii commensurate with those in the mechanically alloyed nano-duplex systems (100 nm – 1 μm) and develop grain boundaries on the order of 10 – 50 nm as observed in systems such as W-Cr and Fe-Mg. The idealized setup is imaged in Figure 2 below. While this model will not yet include grain boundaries, it is hypothesized that meaningful insight into the kinetics of the sintering process can be gained by exploring the different sintering characteristics of positive and negative enthalpy of mixing systems in line with the requirements established for the formation of nano-duplex alloys [1].

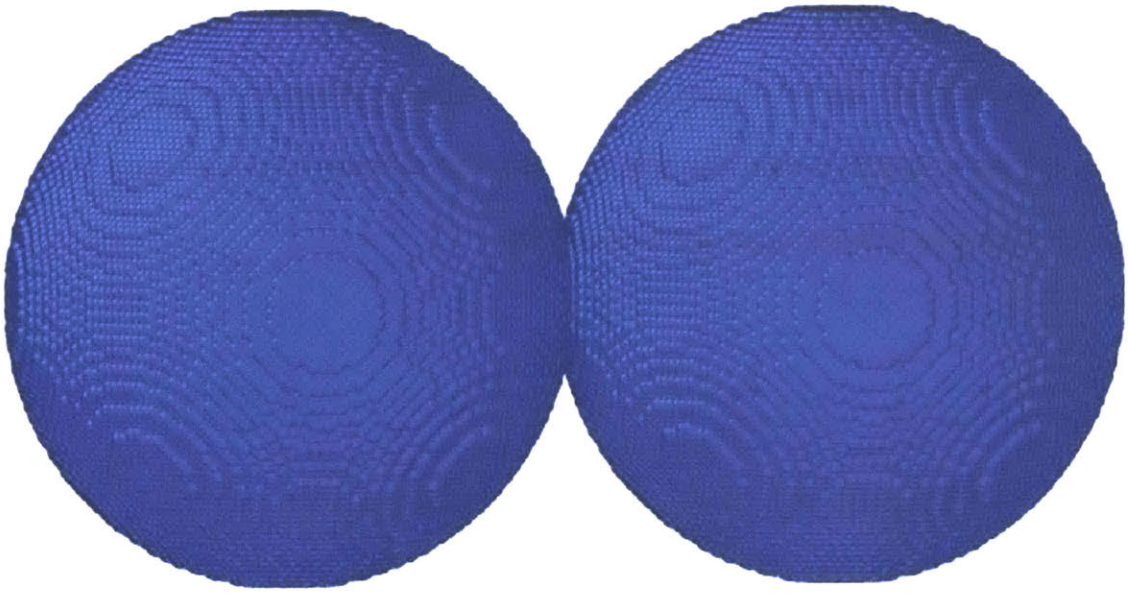

Figure 2: Two particle sintering setup on an FCC lattice; the particles are surrounded by vacancies in this simulation

2 Theoretical Methods

2.1 Rejection Free Kinetic Monte Carlo Algorithm

KMC is an algorithm that samples all possible state transitions in a given system according to Boltzman statistics, while maintaining a rigorously proven time link. This is especially useful for the sintering process because it is fundamentally a diffusion dominated process. This means that it would be difficult to run a purely molecular dynamics simulation and reach the effective timescales required to study the kinetics of the sintering process.

KMC algorithms come in two main flavors, rejection-free KMC and rejection KMC or the standard algorithm. The rejection free algorithm involves calculating all the known transition rates that the system can possibly undergo and subsequently picking from what amounts to a very large weighted distribution via random number generation. As the name implies, all events are accepted, and the total sum of the rates of the system are used to calculate what the residence or dwell time is in real world time to advance the clock after each monte carlo step. This is in effect simulating how long it would take in any given instance for a move to be made anywhere within the system. This also presumes that no two events happen exactly simultaneously, even if they occur in quick succession.

The rejection-based algorithm is a more general case of the rejection free algorithm where it is not necessary to know the rate for each possible transition, but rather the upper bound of rates for the given type of transition that is randomly selected from all possible transitions within any given timestep.

Both algorithms were implemented but the rejection-free algorithm was chosen due to its higher overall computational efficiency compared to its rejection counterpart. More thorough reasons for this decision are outlined in section 3.5. The standard rejection free kinetic Monte Carlo (rfKMC) algorithm employed in this simulation was covered in work by Voter and Bortz et al [30], [31] :

1. Set time $t = 0$
2. Form a list of all possible transitions the system could potentially undergo from the initial state k and number N_k
3. Calculate the rate constants r_{ki} for all possible transitions from state $k \rightarrow i$ and store this in a rate list
4. Calculate the partial sum of the rate list where $n(j) = \sum_{i=0}^{j} r_{ki}$ and $n(j)$ is the j_{th} element of the partial sum
5. Select a random number z on the interval [0,1) and step through the partial sum list until $n(j) > z\, r_{tot}$ where r_{tot} is the last element of the partial sum
6. Implement the chosen transition associated with the j_{th} element of the rate list and update the current state from $k \rightarrow i$
7. Get a new random number z'
8. Update the time with $t = t + \Delta t$ where $\Delta t = (r_{tot})^{-1} \ln\left(\frac{1}{z'}\right)$

A binary search tree was used to efficiently step through the partial sum and search for the condition outlined in step 5. Random numbers were generated using the built in Marseinne Twist random number algorithm (mt19937 under the <random> header) in C++. The overall algorithm was implemented in C++ with post-processing using a combination of Mathematica and Ovito.

Grain boundaries were not included in the model due to system size limitations that will be discussed later in thesis section 3.5. To make this problem more tractable, a lattice KMC simulation was implemented. While this is more granular than a purely atomistic simulation, diffusional processes are well defined events for which the energetics are well understood[32], [33]. This lends itself to the rate calculations required in the Monte-Carlo algorithm, as they can then be parametrized in terms of the local system configuration for increased computational efficiency.

2.2 Rate Calculation

Eyring transition state theory (TST) was used as the basis to compute the rate constant for each evolutionary path of the system[34], [35]. TST posits that the rate of an event is given by the equation:

$$r_i = ve^{-\frac{E_a}{k_b T}} \quad (1)$$

Where E_a is the activation energy for the process, v is the attempt frequency that the system makes from its initial state, and k_b is the Boltzman constant and T is temperature in Kelvin. TST

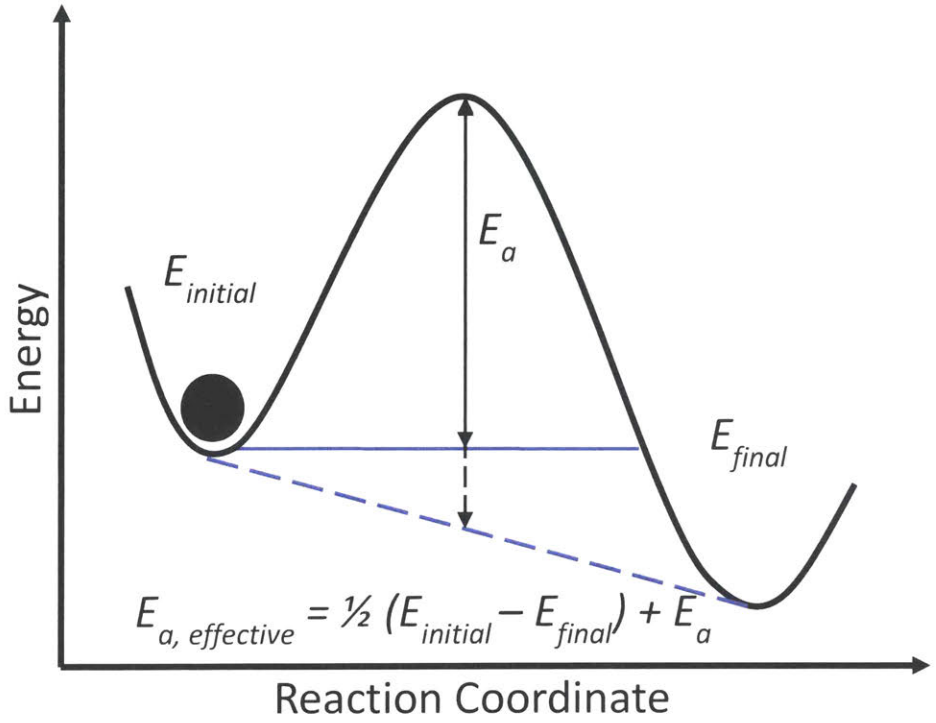

Figure 3: Schematic of the energy landscape for a typical transition. The effective barrier height used in equation (1) is biased by the initial and final energy states of the system.

with Boltzman statistics was chosen to model this system as the rate catalogue will be populated by vacancy mediated diffusion through both the bulk and the surface of the two-particle model. When calculating rates in this model, initial and final conditions of the hopping atom were used to bias the effective barrier height as depicted in Figure 3. A v of 10^{13} was assumed for all transitions.

This was done to minimize the net number of vaporizations in the system. Without biasing for the initial and final state of the system, surface diffusion and de-adsorption would not produce different rate constants within this framework. The energy of the system for a generic configuration was calculated using a bond counting model:

$$E = n_{AA}E_{AA} + n_{BB}E_{BB} + n_{AB}E_{AB} \quad (2)$$

Where n_{xx} represented the number of nearest neighbor bonds of a type X-X. The activation energy for diffusion was taken to be constant and various values were used depending on the composition of the alloy. This type of model has the advantage of being simple enough to capture the enthalpy of mixing of a system using the standard quasi-chemical model:

$$\Delta H = Z\left(-\frac{E_{AA} + E_{BB}}{2} + E_{AB}\right) \quad (3)$$

Where Z is the coordination of the lattice and ΔH is the enthalpy of mixing of the alloy. The cohesive energy per atom of each element normalized by the lattice coordination Z was used to determine bond energies. Heterogenous bonds were calculated using Equation (3) and enthalpy of mixing values from the RKM model compiled within [36].

To simulate systems with well documented bonding energies, Al, Al-Pb, and Al-Sc were chosen. Al-Pb represents a system with a positive enthalpy of mixing, while Al-Sc has a negative enthalpy of mixing. Using the proposed model to simulate these three systems should allow a comparison of the neck formation characteristics under the simple energetics outlined with equations (2) and (3). Two particle samples of each of these systems will be sintered at various temperatures to provide system kinetics as a function of temperature and time. These will be compared with analytical models outlined in later sections.

3 Results and Discussions

3.1 Statement of Results

Under the conditions present in these simulations, positive of enthalpy of mixing systems sintering via vacancy mediated surface and bulk diffusion can allow for the formation of an inter-particle neck dominated by the fastest diffusing element in an alloy. This is one of the pre-requisite conditions for accelerated sintering outlined in [16].

Table 1 : Simulation parameters for tested alloys.

Composition (A-B)	E_{AA} *(eV)*	E_{BB} *(eV)*	E_{AB} *(eV)*	E_a *(eV)*	ΔH *(eV/atom)*
Al	0.283	--	--	0.56	--
Al-Pb	0.283	0.169	0.140	0.56	1.036
Al-Sc	0.283	0.325	0.396	1.0	-1.109

The experimentally reported average of the range of migration energies of Al was used for both the pure aluminum sintering sample and the Al-Pb alloy due to lack of data for Pb migration in aluminum [37]. The activation energy for the Al-Sc alloy was taken to be an average of the activation energies from Al and Sc alloy inter-diffusion work [38] and work in [39] . Cohesive energies were used to estimate the X-X homogenous bond energies by dividing $E_{cohesive}$ by the lattice coordination Z. Cohesive energy values were taken from [40] and were used in conjunction with the enthalpy of mixing values from [36] to calculate X-Y heterogenous bond energies from equation (3).

3.2 Surface Energies

A discussion of surface diffusion dominated sintering is not complete without a quick derivation of the effective surface energy densities that arise from the given energetics. Considering that a nearest-neighbor bond counting model was employed in this simulation, surface energies for the (111) , (110), and (100) atomic planes were calculated. The formula for calculating the energy of a given atomic plane is given by:

$$\gamma_{(hkl)} = E_{(hkl)} \left(\frac{N}{A}\right)_{(hkl)} \tag{4}$$

Where $E_{(hkl)}$ is the bond energy required to create the surface per atom and $\left(\frac{N}{A}\right)_{(hkl)}$ is the areal number density of atoms in the plane (hkl). The geometries of the various planes are given for the FCC lattice below.

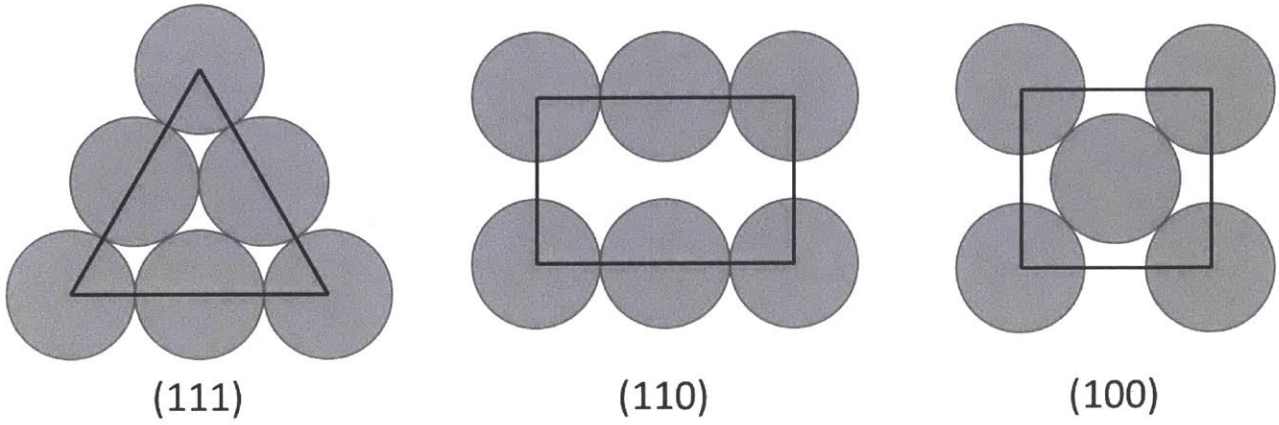

Figure 4: Atomic plane configurations for the FCC lattice

Using these figures, 3, 5, and 4 bonds were broken to form each of the (111), (110), and (100) surfaces respectively. Applying equation (4) to each geometry yields the following set of formulas:

$$\gamma_{(111)} = \frac{12\epsilon}{\sqrt{3}a^2} \tag{5}$$

$$\gamma_{(110)} = \frac{10\epsilon}{\sqrt{2}a^2} \tag{6}$$

$$\gamma_{(100)} = \frac{8\epsilon}{a^2} \tag{7}$$

Equations (5)-(7) are the surface energy densities for each crystallographic plane as a function of the average bond energy ϵ and lattice constant a. Using these equations, surface energies for each plane were calculated for the Al, Al-Sc, and Al-Pb alloys in the table below.

Table 2: Surface energy densities for various alloys and crystallographic planes

Composition	$\gamma_{(111)}\left(\frac{J}{m^2}\right)$	$\gamma_{(110)}\left(\frac{J}{m^2}\right)$	$\gamma_{(100)}\left(\frac{J}{m^2}\right)$
Al	1.92	1.95	2.21
Al-Pb	1.04	1.06	1.20
Al-Sc	2.01	2.05	2.32

Al-Sc and Al-Pb effective bond energies were estimated by assuming that Al-Pb will seek to maximize homogenous bond energies. As such, it was assumed that the effective bond energy was merely the average of the homogenous bond energies for a given broken bond. Al-Sc will attempt to maximize the heterogenous bond, so this value was used to calculate effective surface

energies. It should be noted that these effective bond energies amount to equilibrium atomic configurations, not those exhibited during the evolution of the particle.

The energetics in this model represent a shortcoming in how they reproduce the surface energies of the various alloys and are quite different than those reported in the literature [41]. This model has no relaxation of the surface atoms and only encodes information from the first nearest neighbor. The positive enthalpy of mixing system was assumed to be breaking mainly homogenous bonds while the negative enthalpy of mixing system was assumed to be breaking predominantly heterogenous bonds for the purposes of this calculation.

3.3 Sintering Kinetics

3.3.1 Pure Aluminum

Isothermal sintering simulations for pure aluminum were conducted between 500-1100 K. Particles were simulated with ~ 500,000 atoms and were ~ 20 nm in diameter. Plots of the neck radius vs monte carlo steps and time are shown in Figure 5 (a) and (b) below.

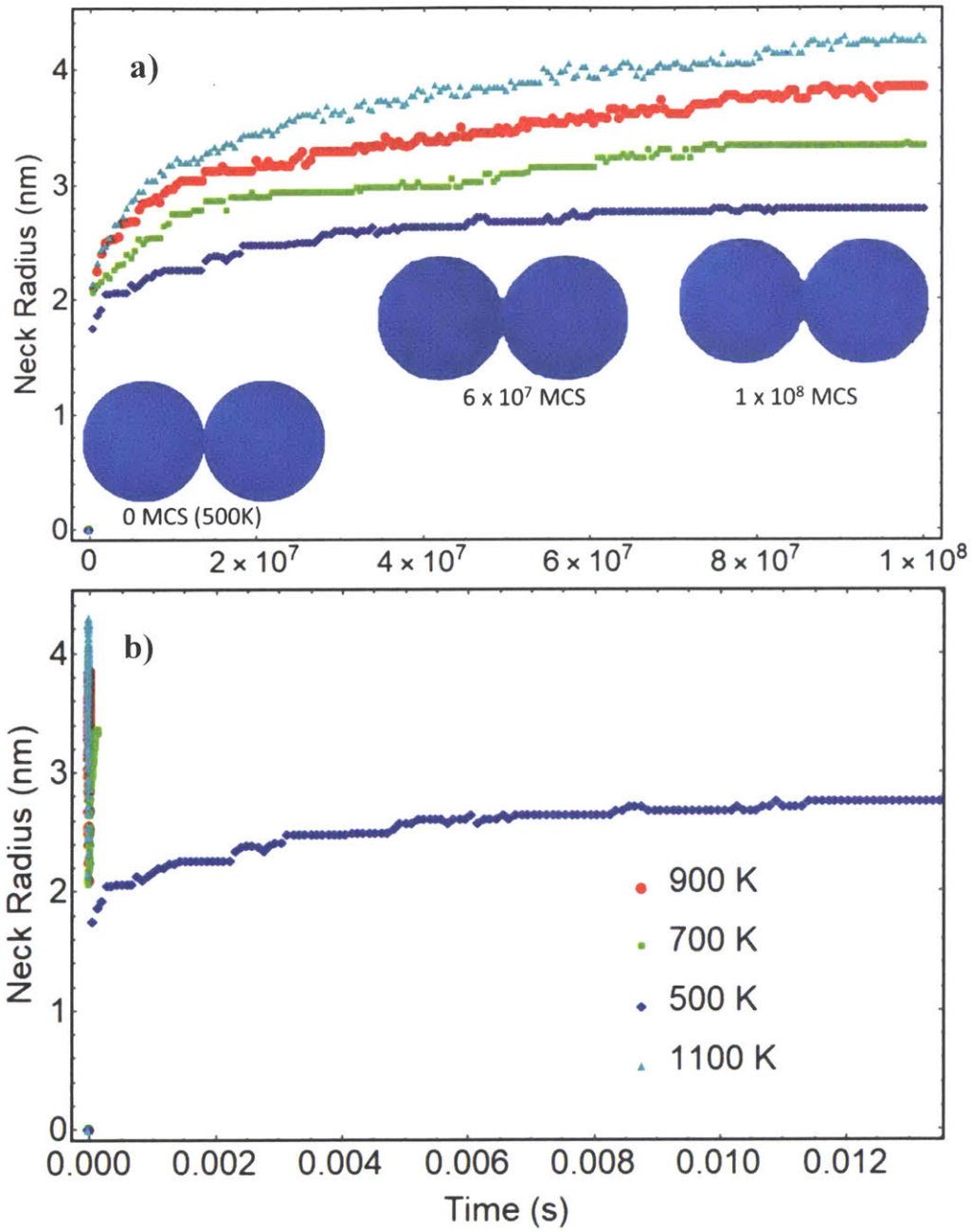

Figure 5: Isothermal neck radius curves for pure aluminum in monte carlo steps (a) and real time (b)

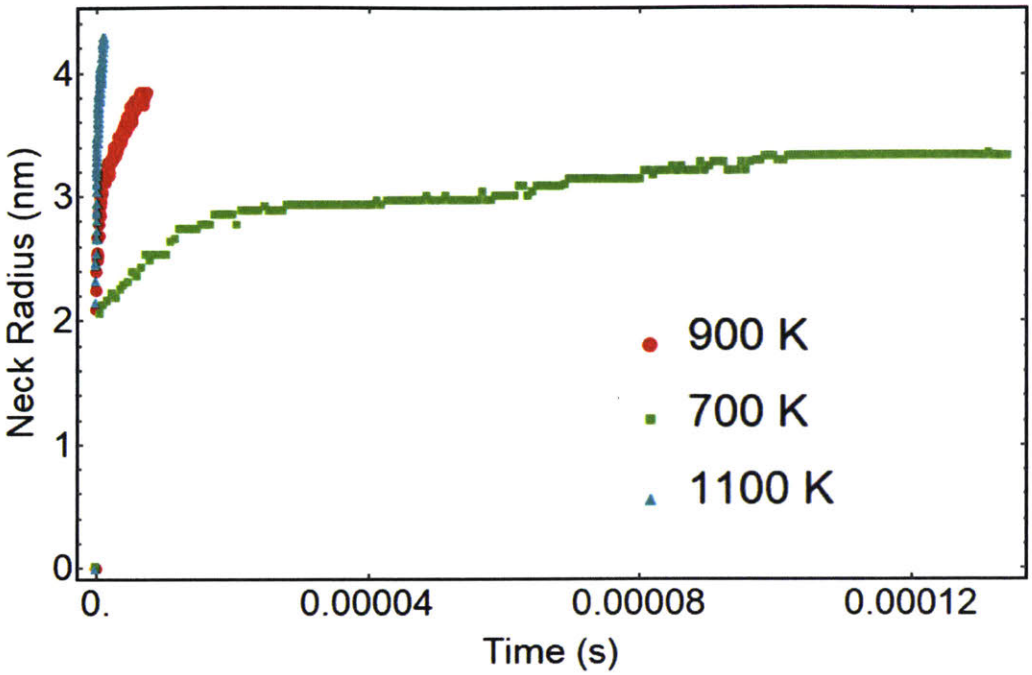

Figure 6: Expanded image of Figure 5b excluding the 500 K isotherm

The model demonstrates that higher heating rates lead to an increase in both the final neck radius and the rate of growth for the neck. In order to assess the accuracy of the time scaling of the model, the neck growth kinetics were compared to a surface diffusion analytical model given in [42]. This is given by the equation:

$$\left(\frac{x}{R}\right)^5 \cong \frac{271\delta D^s \gamma^s \Omega_A}{R^4 kT} t \tag{8}$$

where γ^s is the surface energy, D^s , x is the neck radius, R is the particle radius and δ is thickness. At 500 K, using the vacancy formation energy computed in [39] and an Arrhenius probability of vacancies per lattice site, one finds for a system size of ~500,000 atoms that the expected concentration of vacancies is ~1.17 vacancies for the whole system. It is safe to assume this case corresponds to the pure surface diffusion condition outlined in [42] where $x \propto (t^{1/5})$.

Taking the log of the 500 K data in Figure 5 (b), this analysis is plotted below in Figure 7 and differs from the scaling predicted in equation (4) and that observed from the simulation in the unary, low temperature limit. It is worth noting that to simulate larger system sizes in the future, the time required to reach a given neck size scales as R^4 of the particle.

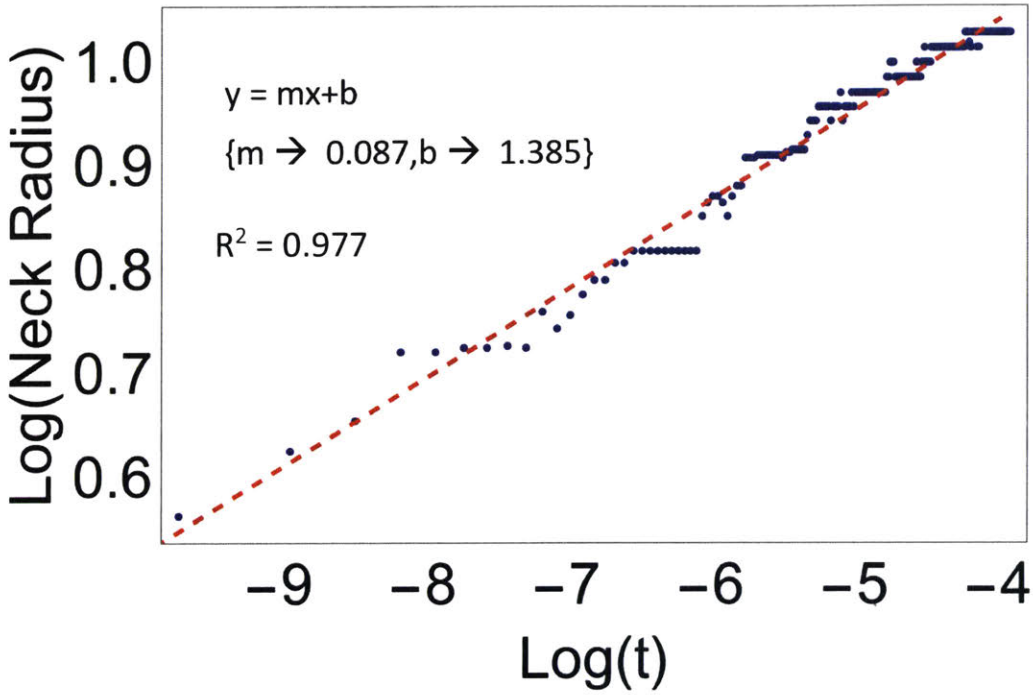

Figure 7: Log of the axes from Figure 4 (b) 500K reveals that the time scaling differs from the analytical predictions outlined in [42]

Advancing this analysis, one can note the deviation from the pure unary aluminum scaling with increasing temperature of the sintering curve as outlined in Figure 8 below. Positive

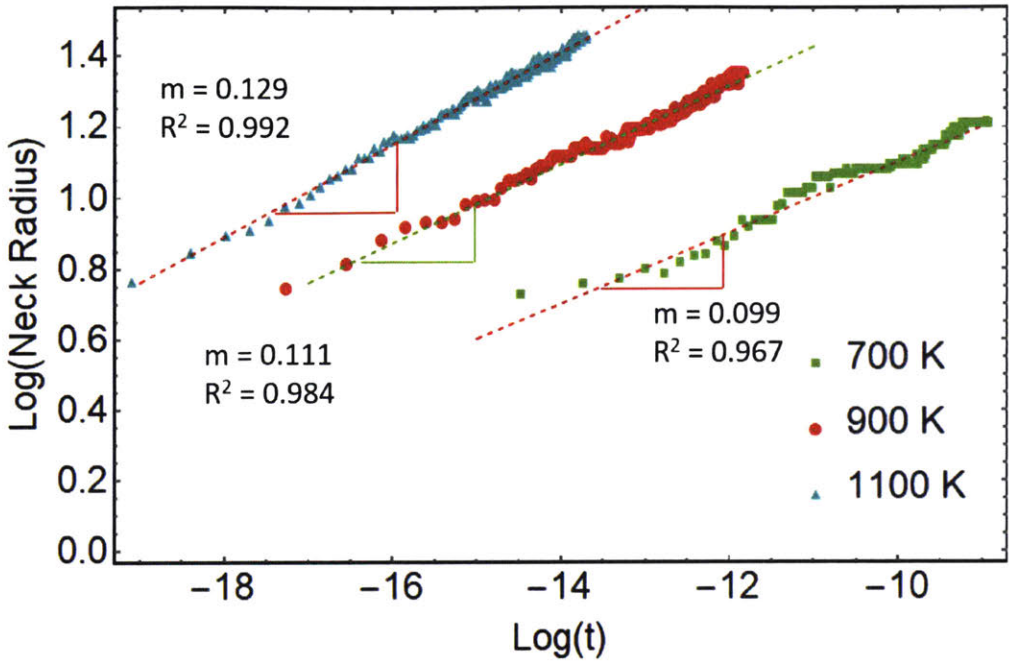

Figure 8: Plot of the neck radius vs time for various unary aluminum neck curves. Note the increasing deviation from ~0.08 power as a function of temperature

deviation in the power law is to be expected, as increasing temperature increases the viability of bulk diffusion, presenting another mechanism by which the inter-particle neck may begin to grow. This increase in bulk diffusion is mediated by the increasing concentration of thermalized vacancies inside of the system. The power law for neck growth deviates increasingly as a function of temperature for each sintering simulation in figure 8 in line with expectations.

3.3.2 Aluminum-Lead

The Al-Pb system sintered at lower temperatures and reached larger neck radii than the pure aluminum sample. This is demonstrated in Figure 9 below. The Al-Pb system has a large positive enthalpy of mixing and exhibited strong phase separation during the sintering process.

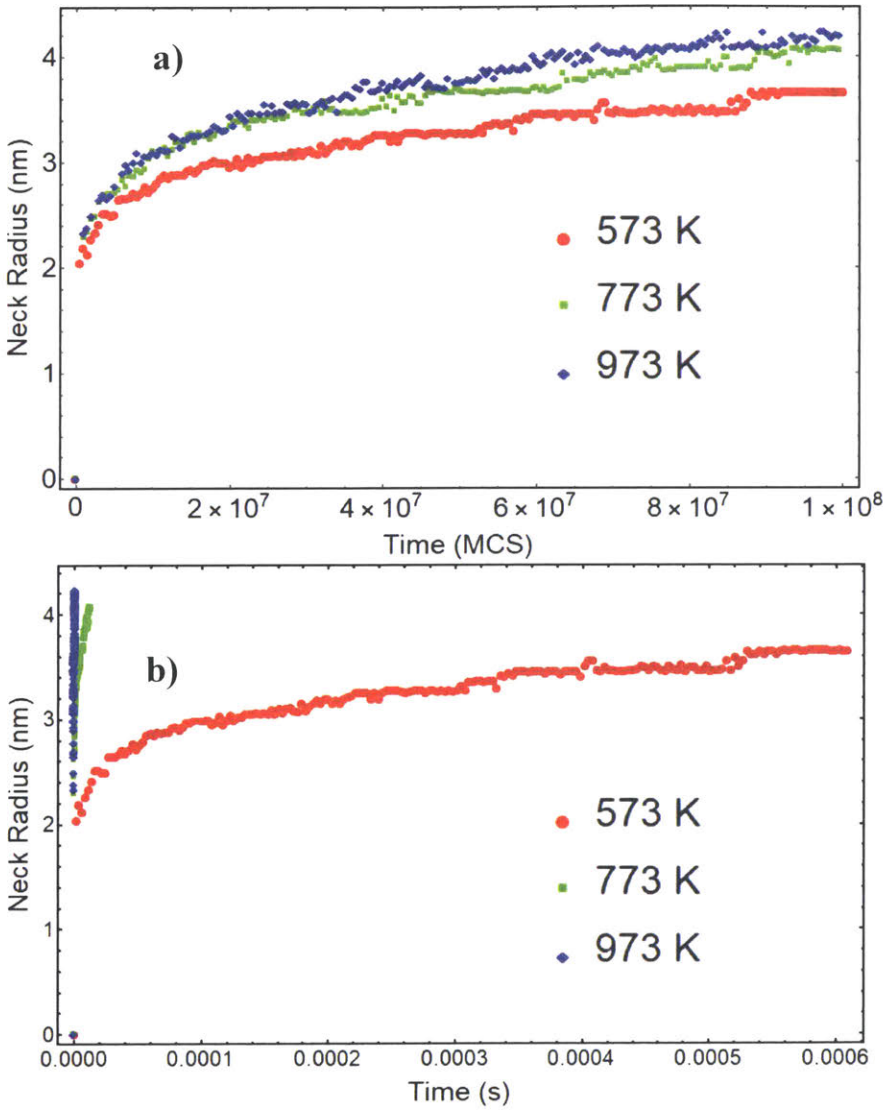

Figure 9: Al-Pb sintering curves for various constant temperature sintering simulations. All compositions tested were 50-50 atomic %.

There are likely two reasons for this. The first is that the cohesive energy of Pb is lower than that of aluminum. This would cause the barrier to diffusional hopping to decrease and the sintering rates calculated throughout the model to increase.

The second is that the positive enthalpy of mixing caused strong phase separation. It is hypothesized that this condition, mirroring that outlined for nano-duplex alloys, allowed for the formation of the neck dominated by the faster diffusing element. This can be seen in images of the sintered particle as a function of the monte carlo time step in Figure 10 below.

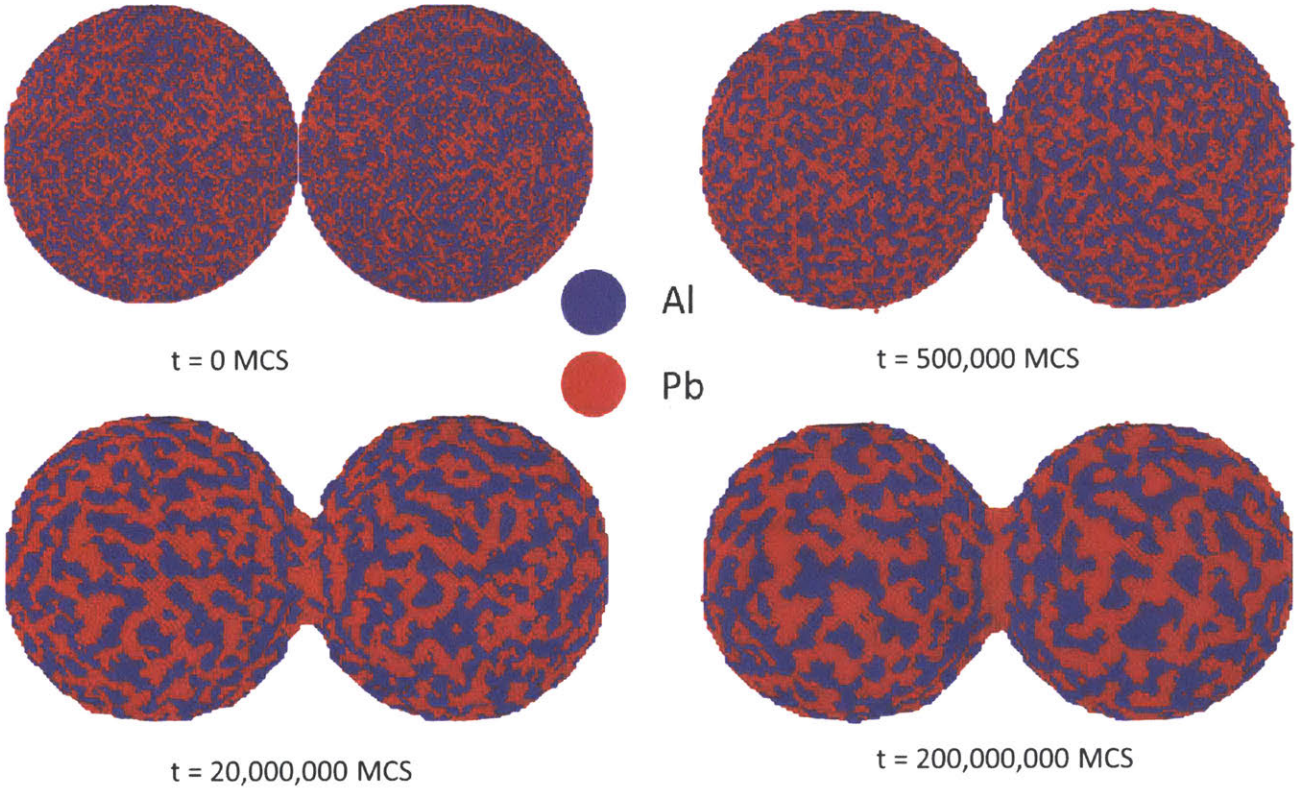

Figure 10:Visualization of Al-Pb sintering at 773 K. Notice the neck growth is dominated by the faster diffusing element which in this case is Pb.

As the neck grew over the course of the simulation, the concentration on the outside of the neck was dominated by Pb, and the interior of the neck formed a pore. This was likely due to a cluster of vacancies within the neck, stabilized by the negative curvature within the region which

allowed for better inter-diffusion with the bulk of the particles in this region. It is theorized that this phase separation allowed for the dominance of the faster diffusing element to drive neck formation and therefore sinter at lower temperatures for shorter cycle durations.

3.3.3 Aluminum-Scandium

The aluminum scandium alloy sintered at higher temperatures than pure aluminum as seen in Figure 11. For similar reasons outlined in the Al-Pb case, it is theorized that this occurred because both because the cohesive energy of Sc is higher than that of aluminum, but also

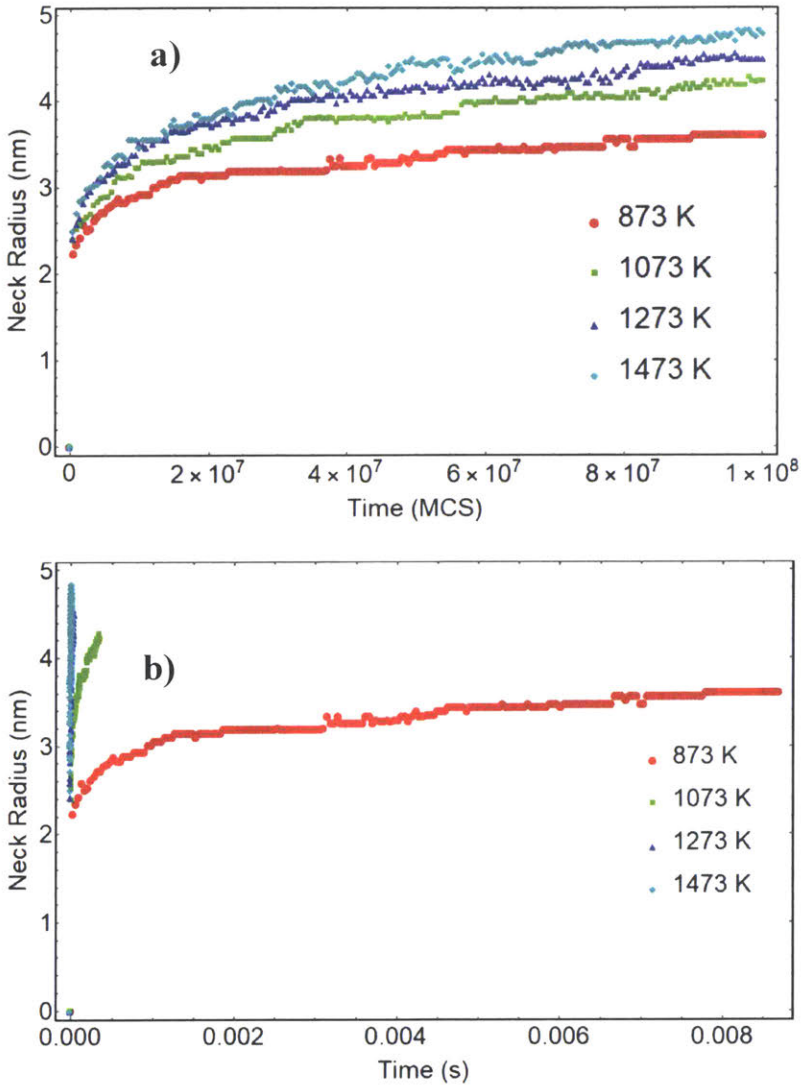

Figure 11: Neck growth curves as a function of Monte Carlo steps (a) and real time (b) in Al-Sc alloy

because this negative enthalpy of mixing system did not allow the faster diffusing element to form the neck.

Figure 12 demonstrates that negative enthalpy of mixing systems does not exhibit neck growth dominated by the faster diffusing element, which in Al-Sc is Al. High enthalpy of mixing seeks to maximize the number of A-B bonds, which in the case of this simple model would cause the formation of an L_{12} structure and one can see evidence of this ordering along the surface of the particle.

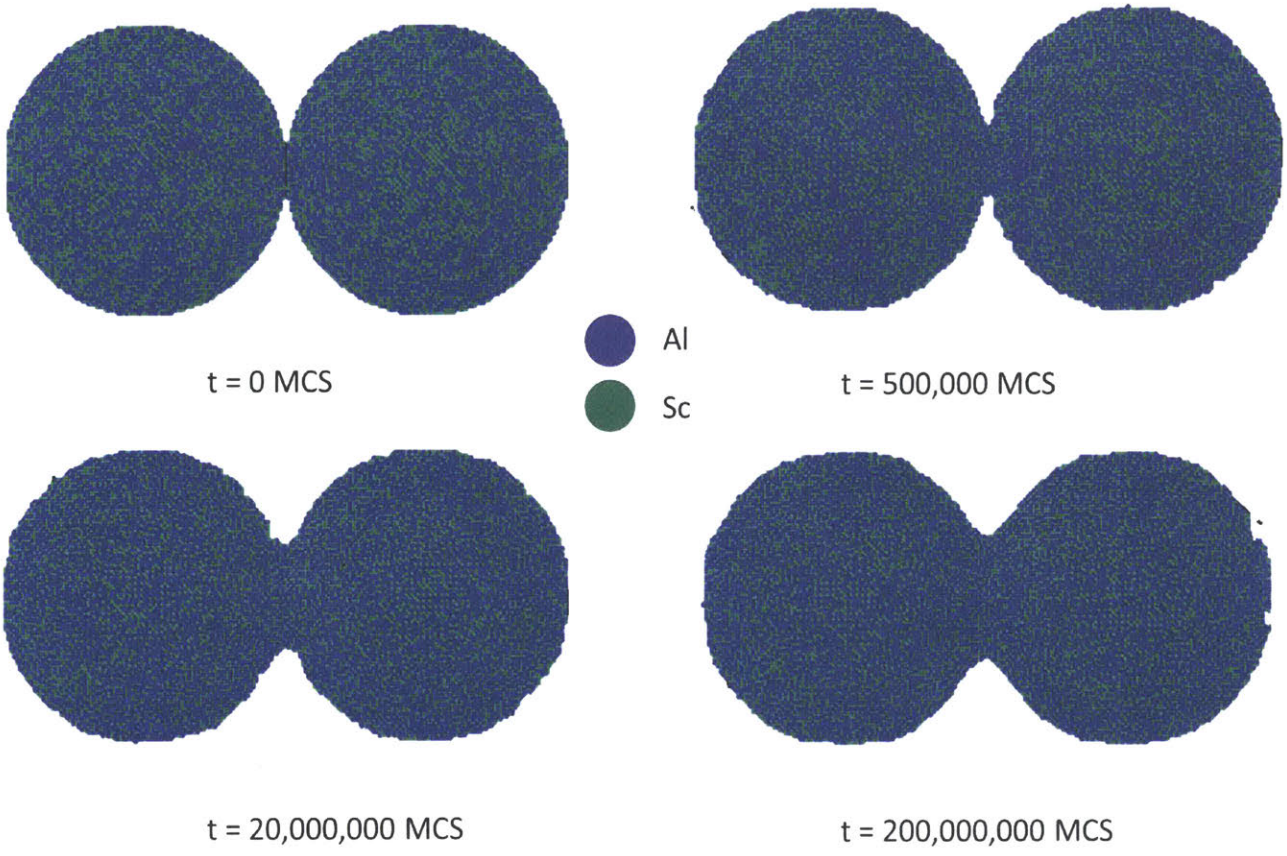

Figure 12: Sintering of Al-Sc alloy (50at% Al , 1273 K) does not exhibit neck growth dominated by the faster diffusing element (Al)

3.4 Sintering Morphology

When examining the criterion for the formation of a nano-duplex, positive enthalpy of mixing is necessary for the solvent phase. The simulations here are philosophically like a nanocrystalline alloy with fast grain boundary diffusion. One in which a large amount of solute decorates the surface (in this case 50 at%) at lower temperatures where grain boundary diffusion dominates the transport of material inside the bulk of the system to the surface [43]. These simulations seem to indicate that for positive enthalpy of mixing systems, the fast diffusing solute atoms are capable of diffusing along the particle surface to form the neck, followed by the diffusion of solvent atoms across the neck to complete the densification process. Of course, more complicated mechanisms are at work in real nanocrystalline systems, including the as-yet unexplained effect of solubility on the diffusion of components across the neck and the subsequent effect this has on the densification rate.

Another unexamined parameter in this project is the surface facet upon which the inter-particle neck forms. Presuming that neck-growth remains roughly on lattice, the surface energies of the crystallographic planes can be quite different, as can the surface diffusion that accompanies them. In this simulation, only growth along the (100) of plane of an FCC lattice was simulated, but it is likely that the kinetics of the sintering process could be altered by the relative orientation of the powder particles, owing to the different surface configurations of the inter-particle necks.

In any case, if one accepts that the positive enthalpy of mixing is necessary for neck formation, and that by including an element that diffuses quickly one can form the neck at lower temperatures than the base element, the smoking gun evidence for nanocrystalline accelerated sintering is if the diffusion along the grain boundaries can decorate the surface with enough

solute to drive the neck formation. This is one of the main objectives for any future work in this area when simulation size and computational limitations are overcome.

3.5 Simulation Size and Limitations

The current simulation size consists of ~500,000 atoms with two particles that each have a 20 nm diameter (using the pure aluminum lattice constant). The original goal was to simulate 100 nm to 1 μm in diameter particles with grain sizes in the 10-30 nm range to help develop a precise kinetic criterion for accelerated sintering in nano-duplex systems. This would mean the system size would range from 100 million to 100 billion atoms.

These larger system sizes represent both memory and computation speed challenges for KMC. Fully densified FCC and BCC lattice representations can be developed (and for FCC have been) to ensure that the lattice alone fits within a reasonable amount of memory. Compounding this issue is that both the kinetic monte carlo rate list and partial sums would need to be a vector of floating point numbers that would have at least 12 entries for each atom accounting for all the potential hopping directions in the FCC lattice (and 8 for BCC) which would create large memory demands.

The evaluation time of very large partial sums and rate lists was addressed in this code by attempting to implement local updating so that only the effected elements after each diffusional hop (i.e. adjacent atoms now having a different neighbor configuration) would be updated in the rate list. However, in every step, the partial sum needed to be re-calculated at least from the last known position from which the first element changed.

Attempts were made to use the rejection kinetic Monte Carlo algorithm also known as the standard algorithm[44]. However, rejection of each time step is dependent on the upper bound rate of the system for any given transition, which in this case can range up to 3 orders of magnitude (from complete de-adsorption to adsorption). This makes the rejection algorithm inefficient on top of the fact that the upper bound rate effectively evolves as different diffusion mechanisms predominate during the sintering process (including bulk, grain boundary, and surface diffusion).

The list of available atoms for movement selection is small and constantly changing. This presents one more degree of complexity for sintering systems in a KMC simulation compared to their metropolis counterparts. To save time on the rate list and partial sum, one could attempt to keep track of only those atoms which are adjacent to a vacancy, which in the case of the simulations executed in this system, amount to ~2% of the atoms. This would decrease the rate list, decrease the partial sum list, and thereby decrease both memory demand and the computational speed between each timestep

However, this presents a memory management problem as the list of atoms adjacent to vacancies fluctuates continuously throughout the simulation (it has been noted to grow as high as 3% and as low as 1%). Using vector memory management in C++ would result in frequent resizing and memory re-allocation, which would likely cause a dramatic performance hit. Couple this with the evolution of the system and the movement of atoms into and out of configurations where they are adjacent to vacancies and the difficulty in maintaining a fast, memory efficient look-up table is also a challenge for future work.

Other possible optimization techniques include having a lattice that can successfully fit in the L3 cache of the processor. One could attempt to to address this by addressing atomic

composition within an individual byte to decrease memory foot-print and store more of the lattice within the system cache. One could also alter the address scheme to address lattice sections in 16 x 16 x 16 cubes, which should create 4096 KB of data mapping to the exact standard page size in both Windows and Linux. These optimizations would certainly be helpful if the code is exhibiting a high percentage of cache misses. Analysis of the code used in this simulation with Valgrind, an open source cache-miss evaluation software that can deduce how memory starved simulations are, demonstrated that L1 cache misses occurred with a 0% rate and L3 cache misses occurred at a rate of 6.2%. While not perfect, this result seems to suggest that optimizations may not result in dramatic performance increases.

4 Conclusion and Future Work

The effect of enthalpy of mixing on the sintering of small particles was explored. It was determined that under the conditions in this model, positive enthalpy of mixing systems sintered more quickly than their unary or negative enthalpy of mixing counterparts. This was due both to differences in cohesive energy of the alloying elements as well as the ability of the positive enthalpy of mixing system to form a neck predominated by the fast diffusing element more quickly for a given temperature than their unary or negative enthalpy of mixing counterparts. The next step to exploring sintering of nanocrystalline alloys would be to include grain boundary diffusion and to begin testing alloy compositions with much lower concentrations of the solute. This will hopefully yield the necessary insight to produce an analytical criterion for whether a particular alloy will exhibit accelerated sintering as well as form stable nanocrystalline grains.

5 References

[1] A. R. Kalidindi and C. A. Schuh, "Stability criteria for nanocrystalline alloys," *Acta Mater.*, vol. 132, pp. 128–137, Jun. 2017.

[2] M. Park and C. A. Schuh, "Accelerated sintering in phase-separating nanostructured alloys," *Nat. Commun.*, vol. 6, no. 1, p. 6858, Dec. 2015.

[3] E. Zhou, C. Suryanarayana, and F. H. S. Froes, "Effect of premilling elemental powders on solid solubility extension of magnesium in titanium by mechanical alloying," *Mater. Lett.*, vol. 23, no. April, pp. 27–31, 1995.

[4] C. C. Koch, "Materials Synthesis by Mechanical Alloying," *Annu. Rev. Mater. Sci.*, vol. 19, no. 6, pp. 121–143, 1989.

[5] H. Gleiter, "Nanocrystalline Materials," *Prog. Mater. Sci.*, vol. 33, pp. 223–315, 1990.

[6] R. Z. Valiev, R. K. Islamgaliev, and I. V Alexandrov, "Bulk nanostructured materials from severe plastic deformation," *Prog. Mater. Sci.*, vol. 45, no. 2, pp. 103–189, 2000.

[7] C. Suryanarayana, "Nanocrystalline Materials," *Int. Mater. Rev.*, vol. 40, no. 2, pp. 41–64, 1995.

[8] R. Z. Valiev, R. K. Islamgaliev, and I. V Alexandrov, "Bulk nanostructured materials from severe plastic deformation," *Prog. Mater. Sci.*, vol. 45, no. 2, pp. 103–189, 2000.

[9] C. C. Koch, R. O. Scattergood, K. M. Youssef, E. Chan, and Y. T. Zhu, "Nanostructured materials by mechanical alloying: new results on property enhancement," *J. Mater. Sci.*, vol. 45, no. 17, pp. 4725–4732, 2010.

[10] Z. Cordero *et al.*, "Powder-Route Synthesis and Mechanical Testing of Ultrafine Grain Tungsten Alloys," *Metall. Mater. Trans. A*, vol. 45, no. 8, pp. 3609–3618, 2014.

[11] T. Chookajorn, H. Murdoch, and C. A. Schuh, "Design of stable nanocrystalline alloys," *Science (80-.).*, vol. 337, no. 6097, pp. 951–954, 2012.

[12] H. A. Murdoch and C. A. Schuh, "Stability of binary nanocrystalline alloys against grain growth and phase separation," *Acta Mater.*, vol. 61, no. 6, pp. 2121–2132, 2013.

[13] T. Chookajorn and C. A. Schuh, "Nanoscale segregation behavior and high-temperature stability of nanocrystalline W–20 at.% Ti," *Acta Mater.*, vol. 73, pp. 128–138, 2014.

[14] C. Suryanarayana, "Mechanical alloying and milling," *Prog. Mater. Sci.*, vol. 46, no. 1–2, pp. 1–184, 2001.

[15] Y. Z. Chen *et al.*, "Nanocrystalline Fe–C alloys produced by ball milling of iron and graphite," *Acta Mater.*, vol. 61, no. 9, pp. 3172–3185, May 2013.

[16] M. Park and C. A. Schuh, "Accelerated sintering in phase-separating nanostructured alloys," *Nat. Commun.*, vol. 6, 2015.

[17] M. Park, T. Chookajorn, and C. A. Schuh, "Nano-phase separation sintering in

nanostructure-stable vs. bulk-stable alloys," *Acta Mater.*, vol. 145, pp. 123–133, Feb. 2018.

[18] C. Suryanarayana, "Mechanical alloying and milling," *Prog. Mater. Sci.*, vol. 46, no. 1–2, pp. 1–184, 2001.

[19] M. P. D. M. I. of T. Park, "Design of bulk nanocrystalline tungsten alloys via nano-phase separation sintering," 2015.

[20] J. D. Hansen, R. P. Rusin, M.-H. Teng, and D. L. Johnson, "Combined-Stage Sintering Model," *J. Am. Ceram. Soc.*, vol. 75, no. 5, pp. 1129–1135, May 1992.

[21] H. Zhu, "Sintering processes of two nanoparticles: A study by molecular dynamics simulations," *Philos. Mag. Lett.*, vol. 73, no. 1, pp. 27–33, Jan. 1996.

[22] K. Chockalingam, V. G. Kouznetsova, O. van der Sluis, and M. G. D. Geers, "2D Phase field modeling of sintering of silver nanoparticles," *Comput. Methods Appl. Mech. Eng.*, vol. 312, pp. 492–508, Dec. 2016.

[23] Y. U. Wang, "Computer modeling and simulation of solid-state sintering: A phase field approach," *Acta Mater.*, vol. 54, no. 4, pp. 953–961, Feb. 2006.

[24] M. R. Dorr, J.-L. Fattebert, M. E. Wickett, J. F. Belak, and P. E. A. Turchi, "A numerical algorithm for the solution of a phase-field model of polycrystalline materials," 2009.

[25] F. Y. Wu, "The Potts model," *Rev. Mod. Phys.*, vol. 54, no. 1, pp. 235–268, Jan. 1982.

[26] F. Qiu, T. A. Egerton, and I. L. Cooper, "Monte Carlo simulation of nano-particle sintering," *Powder Technol.*, vol. 182, no. 1, pp. 42–50, Feb. 2008.

[27] A. Violi, A. F. Sarofim, and G. A. Voth, "KINETIC MONTE CARLO–MOLECULAR DYNAMICS APPROACH TO MODEL SOOT INCEPTION," *Combust. Sci. Technol.*, vol. 176, no. 5–6, pp. 991–1005, May 2004.

[28] S. Hara, A. Ohi, and N. Shikazono, "Sintering analysis of sub-micron-sized nickel powders: Kinetic Monte Carlo simulation verified by FIB–SEM reconstruction," *J. Power Sources*, vol. 276, pp. 105–112, Feb. 2015.

[29] T. H. Lim, D. Mccarthy, S. C. Hendy, K. J. Stevens, S. A. Brown, and R. D. Tilley, "Real-Time TEM and Kinetic Monte Carlo Studies of the Coalescence of Decahedral Gold Nanoparticles," *ACS Nano*, vol. 3, no. 11, pp. 3809–3813, 2009.

[30] A. F. Voter, "INTRODUCTION TO THE KINETIC MONTE CARLO METHOD," in *Radiation Effects in Solids*, Dordrecht: Springer Netherlands, pp. 1–23.

[31] A. B. Bortz, M. H. Kalos, and J. L. Lebowitz, "A new algorithm for Monte Carlo simulation of Ising spin systems," *J. Comput. Phys.*, vol. 17, no. 1, pp. 10–18, Jan. 1975.

[32] G. Henkelman, B. P. Uberuaga, and H. Jónsson, "A climbing image nudged elastic band method for finding saddle points and minimum energy paths," *J. Chem. Phys.*, vol. 113, no. 22, p. 9901, Nov. 2000.

[33] H. JÓNSSON, G. MILLS, and K. W. JACOBSEN, "Nudged elastic band method for

finding minimum energy paths of transitions," in *Classical and Quantum Dynamics in Condensed Phase Simulations*, 1998, pp. 385–404.

[34] H. Eyring, "The Activated Complex in Chemical Reactions," *J. Chem. Phys.*, vol. 3, no. 2, pp. 107–115, Feb. 1935.

[35] M. R. Marcelin, "Contribution à l'étude de la cinétique physico-chimique," *Ann. Phys. (Paris).*, vol. 9, no. 3, pp. 120–231, Apr. 1915.

[36] H. A. (Heather A. Murdoch, "Design of a stable nanocrystalline alloy," 2013.

[37] W. Szkola, / I., W. Opolu, and Z. Fieyki, "Vacancy Migration Energy in Aluminium as Determined from Exoelectron Emission Measurements l)."

[38] R. W. Hyland, "Homogeneous Nucleation Kinetics of AI3Sc in a Dilute AI-Sc Alloy."

[39] M. J. Gillan, "Calculation of the vacancy formation energy in aluminium," *J. Phys. Condens. Matter*, vol. 1, no. 4, pp. 689–711, Jan. 1989.

[40] C. Kittel, *Introduction to solid state physics*. Wiley, 2005.

[41] N. E. Singh-Miller and N. Marzari, "Surface energies, work functions, and surface relaxations of low-index metallic surfaces from first principles," *Phys. Rev. B*, vol. 80, no. 23, p. 235407, Dec. 2009.

[42] W. Coblenz, J. Dynys, and R. Coble, "Initial stage solid state sintering models. A critical analysis and assessment," *Sinter. Process. Mater. Sci. Res.*, vol. 13, pp. 141–157, 1980.

[43] Y. Chiang, D. P. Birnie, and W. D. Kingery, *Physical ceramics*. J. Wiley, 1997.

[44] S. A. Serebrinsky, "Physical time scale in kinetic Monte Carlo simulations of continuous-time Markov chains," *Phys. Rev. E*, vol. 83, no. 37701, 2011.